The effects of rainfall on groundwater hydrogeochemistry and chemical weathering

Xinhui He
China University of Geosciences School of Environmental Studies
Hong Zhou
China University of Geosciences School of Environmental Studies
Junwei Wan (wanjw@cug.edu.cn)
China University of Geosciences School of Environmental Studies
Yuan Guo
China University of Geosciences School of Environmental Studies
Heng Zhao
China University of Geosciences School of Environmental Studies

Research Article

Keywords: High-resolution monitoring, Chemical weathering, Hydrogeochemical processes, Rainfall, Carbonate rock, Evaporite, End-member mixing

Posted Date: May 12th, 2022

DOI: https://doi.org/10.21203/rs.3.rs-1548512/v1

Abstract

Due to the special hydrogeological conditions in karst areas, groundwater responds quickly to rainfall. The covariation of ion concentrations and spring discharge during rainfall can help us better understand the hydrogeochemical process of groundwater occurring in the heterogeneous karst aquifers. In this study, high-resolution monitoring of groundwater runoff, hydrochemistry, and stable isotopes were conducted at the Qingjiangyuan (QJY), the source of the Qingjiang River catchment in Hubei, China. The purpose is to investigate the changes in hydrogeochemical processes and chemical weathering under the influence of rainfall. The dynamics of spring discharge indicates the presence of multiple medium such as pipelines and fissures in the aquifer. Pearson correlation analysis shows that the main sources of the solute in the QJY are carbonate minerals (mainly calcite and dolomite), evaporites (mainly gypsum and sylvite), celestite and strontianite. Anthropogenic activities have less impact on groundwater solutes. Although carbonate minerals dominate the hydrochemistry, the changes in hydrogeochemical behavior caused by rainfall may come from gypsum, which is supported by the ion concentrations. The results suggest that both carbonate rocks and evaporites have important roles in hydrochemistry. Therefore, we assume that the dissolved cations in groundwater come from rain, carbonate rock and evaporite weathering. The contributions of these three end-members were quantified based on the law of mass conservation. The proportions of carbonate weathering and evaporite weathering were 83.4% (85.2%-80.3%) and 11.6% (6.9%-18.0%), respectively, and rain was 5.0% (0.1%-10.4%). These results were integrated into a hydrogeological conceptual model that explain the observed hydrogeochemical processes, including rock weathering, piston and dilution effects caused by rainfall. The proposed conceptual model helps to improve the understanding of hydrogeochemical processes and chemical weathering in karst areas.

1. Introduction

Karst water plays an important role in global water resources, with approximately 25% of the world's population relying on karst water as a source of drinking water (White 2002; Bakalowicz 2005). Karst aquifers are highly heterogeneous due to irregular connections of karst pipelines and fissures (Herman et al, 2009; Frank et al, 2019). Rainwater is the main source of karst groundwater, so karst groundwater systems are sensitive to rainfall, especially in the karst region of South China (Hu et al, 2008; Kurtulus et al, 2010; Luo et al, 2017). Therefore, an intensive study of the hydrological and hydrochemical variations under the influence of rainfall is helpful for the conservation and management of karst groundwater resources (Zhao et al, 2010; Li et al, 2016).

Daily or monthly hydrological, hydrochemical, and isotopic variations obtained through long-term monitoring facilitate the understanding of the response of hydrological processes at different temporal and regional scales (Doctor et al, 2006; Darling et al, 2016). High-resolution monitoring can reflect the subtle dynamics of recharge behavior and can explain hydrogeochemical processes (Pu et al, 2011; Gassen et al, 2017). Rainfall events can stimulate a variety of changing behaviors in hydrodynamics and hydrogeochemistry. The use of high-resolution monitoring methods in the study of the karst water system

response to rainfall can achieve better results. In the study of karst underground rivers in southwest China, Jiang (2018) found that rainfall transported sulfuric acid and nitric acid introduced by urbanization to groundwater, which changed the hydrological process of groundwater and interfered with the carbon cycle.

Many studies characterized groundwater-bearing medium by revealing the attenuation of spring discharge during rainfall (Zhou et al, 2019). The studies of Wang (2021) and Chang (2021) showed that karst development can be determined based on spring discharge attenuation, and the proportion of different water-bearing medium can also be calculated. The hydrogeological characteristics of groundwater in different medium are prerequisites for hydrogeochemical behavior (Luo et al, 2016). Fresh rainwater enters underground and is efficiently recharged and transported through pipelines. The spring is a mixture of fast flow and matrix flow, and the groundwater in the matrix will be collected in the pipelines (Perrin et al, 2003; Jiang et al, 2018). The proportion of fast flow and matrix flow mixing in groundwater determines the dynamics of ion concentration and spring discharge. Therefore, the transportation of rainwater into the ground causes a covariation in ion concentration and spring discharge. Therefore, the combination of spring discharge, hydrochemistry and stable isotopes can provide a better understanding of the hydrogeochemical mechanisms in hydrological perspective (Nisi et al, 2008; Wang et al, 2021).

Elemental fractionation occurs during water-rock reactions and stable isotopes can trace hydrogeochemical processes and quantify the contribution of different sources in the hydrochemical evolution (Meredith et al, 2009; Sun et al, 2021). In fact, the mixture of different potential sources, such as rain, carbonate rocks, silicate rocks, evaporites and anthropogenic input contribute significantly to the solutes in water (Millot et al, 2003; Moon et al, 2007; Zhang et al, 2019). However, anthropogenic input of SO_4^{2-} and Cl^- may lead to misestimation of the effect of evaporite weathering. Water quality monitoring at QJY showed high SO_4^{2-} concentration in groundwater, which is more likely to originate from gypsum (one of the evaporite minerals). Although some studies used stable isotopes to quantify SO_4^{2-} produced by evaporites, they did not emphasize the influence of evaporites on groundwater in karst areas that contained evaporites. In this study, high-resolution monitoring of macroelements and Sr were used to quantify the influence of evaporites and revealed the transport characteristics of evaporite minerals. The purposes of this study are (1) understand the dynamics of hydrochemistry and karst spring discharge and its causes; (2) identify groundwater solute sources and calculate their proportion; (3) analyze the variations in hydrogeochemical behavior and chemical weathering under the influence of rainfall and discuss its mechanisms.

2. Hydrogeological Background Of The Study Area

The Qingjiang River is the second largest tributary of the Yangtze River in Hubei Province, and its source is also called the Qingjiangyuan (QJY). The QJY is located at the foot of the Qiyue Mountain on the northeastern edge of the Wuling Mountain area, with a spring outcrop height of 1220 m. The study area has a subtropical monsoon climate with an average annual temperature of 15.2°C. There is abundant

precipitation in the study area, with an average annual rainfall of 1561 mm, which is concentrated from April to September, accounting for 70% of the annual precipitation (Chen et al, 2012; Sun et al, 2016).

The distribution of strata in the study area is controlled by the Qiyue Fold, and dips 20°-40° to the east. The strata exposed from old to new are: the lower Permian formation (P_1), the upper Permian formation (P_2), the Triassic Daye formation (T_1d), the Jialingjiang formation (T_2j) and the Badong formation (T_2b) (Fig. 1). The upper Permian formation (P_2) and the Triassic Badong formation (T_2b) are mudstones and shales. The lower Permian formation (P_1) and the Triassic Daye formation (T_1d) are carbonate rocks, while the Triassic Jialingjiang formation (T_2j) is carbonate rocks and evaporites (Xu et al, 2004). The paleoclimatic environment during the deposition of the Triassic Jialingjiang formation (T_2j) was hot and arid (Li et al, 2020). Therefore, the minerals in the Jialingjiang formation are mainly composed of calcite, dolomite, gypsum, sylvite, and minor amounts of celestite and strontianite (Wang et al, 2022).

QJY is developed in the Triassic Jialingjiang formation, which is one of the water sources for residents in the surrounding area, with less pollution and excellent water quality. The elevation of the recharge area is 1300–1500 m, and most of the recharge area is trough valleys, including the surrounding depressions and the mountain slope. The soil on the slopes is thin, generally less than 0.5 m, and carbonate rocks are exposed in some steep terrain; the thickness of soil in the depressions is more than 1 m, and almost all the flat areas are reclaimed for farmland, planting corn, tobacco and so on. There is an underground river entrance (LLD) at a distance of 5.4 km to the south of the QJY, which recharges the aquifer during rainfall and breaks off when there is no rain.

3. Materials And Methods

Groundwater levels (with a resolution of 0.001 m), temperature (with a resolution of 0.1°C) and conductivity (EC, with a resolution of 0.1 μS/cm) are continuously monitored at the QJY with an automated field meter (Model 3001 LTC Levelogger, Solinst Canada Ltd.). Groundwater monitoring began in November 2019 and ended in November 2021 for two hydrologic years at a frequency of one hour. The spring discharge was obtained according to the regression equation (Eq. 1):

$$Q = 3.833*h*\left(\frac{6h-0.6}{4h+5.6}\right)^{\frac{2}{3}} \quad \text{Eq.}(1)$$

where Q is discharge (L/s); and h is monitored water level (m).

The rainfall data were obtained from a tipping-bucket rain-gauge, which was installed on the roof of a building near the QJY, with a resolution of 0.2 mm. Portable water quality parameter analyzer (PH828, SMART SENSOR) was used to measure groundwater pH (with a resolution of 0.01 pH units) in the field.

Hydrochemistry and stable isotopes monitoring were conducted from 09:30 on July 10, 2021 to 07:30 on July 15, 2021, during which rainfall occurred. Samples were collected every 2 hours, encrypted to 1 hour

after the rainfall started, and the sampling frequency resumed after the rainfall stopped for 24 hours. During the monitoring process, 73 groundwater and 1 rainwater samples were collected and tested within 2 weeks. Clean polyethylene (HDPE) bottles were rinsed 3 times with the collected groundwater before collection and to ensure that no bubbles were left in the bottles. All samples were filtered through a 0.45 μm acetate fiber membrane filters. The bottles for cation analysis were acidified to pH less than 2 with ultra-purified HNO_3, and samples were stored in a refrigerator at 4°C before laboratory analysis.

Cations were analyzed by ICP-OES (iCAP7600, Thermo Fisher Scientific, USA), and anions were analyzed by ion chromatography (IC-2200, Thermo Fisher Scientific, USA), with a resolution of 0.001 mg/L for all ions. In the sample analysis, 10% of the samples were selected as parallel samples. HCO_3^- was measured by the potentiometric titrimetric method, and each sample was titrated three times with an average error less than 5%. The normalized index of charge balance (NICB) for all samples was within ± 5%, which indicates that the sample quality is acceptable. Stable hydrogen-oxygen isotopes were measured by a liquid isotope analyzer (IWA-45EP, LGR), the results were expressed by $\delta^{18}O$ (with an accuracy of 0.1‰) and δD (with an accuracy of 0.5‰) of the international standard V-SMOW (Vienna Standard Mean Seawater). The analysis of cations, anions and stable hydrogen-oxygen isotopes was completed in the Geological Survey Experimental Center of China University of Geosciences (Wuhan). The saturation index (SI) of calcite, dolomite, gypsum, celestite and strontianite in groundwater was calculated by using PHREEQC Interactive 3.0 software.

4. Results

4.1 Temporal variations of spring discharge, temperature and conductivity in the QJY

High resolution monitoring (2019.11-2021.11) of runoff in the QJY showed that spring flows responded rapidly to rainfall events. Spring discharge increased within 3–7 hours after the rainfall began and recovered after 5–7 days (Fig. 2). The increase in spring discharge at the QJY generally occurred after continuous rainfall or rainfall intensity larger than 8 mm/h. It is obvious that there are seasonal variations in spring discharge, which is much higher in summer (from June to August) than in winter (from December to February). The spring discharge in summer remained approximately 400 L/s and reached a maximum of 6030 L/s after the rain (July 16, 2020). In contrast, the spring discharge is about 200 L/s and the maximum is only 1774 L/s (January 7, 2020) in winter with less rainfall.

Groundwater temperature in the QJY was consistent with seasonal variations, with an average temperature of 11.7°C in winter and 12.4°C in summer. It should be noted that the influence of rainfall on groundwater temperature cannot be ignored, which recharges warm in summer and cold in winter. The rainfall causes the groundwater temperature rise in summer, but the fluctuation in temperature is less than 1°C, which may be related to the control of the surrounding rock.

The EC at the outlet of the QJY was ~ 200 μs/cm and lower in summer than other seasons. In contrast to the spring flow, the EC exhibited a rapid decrease followed by a slow increase after the rainfall started, and the EC decreased to 120 μs/cm under the influence of continuous rainfall (maximum rainfall intensity of 13 mm/hour) from July 28 to August 7, 2020. The rapid decrease of EC was caused by rainwater entered underground through ponors or fissures and diluted groundwater. However, the response of EC to rainfall was 4 ~ 5 h later than that of spring discharge, which was attributed to the difference in pressure conduction and solute transportation.

4.2 Responses of spring discharge, hydrochemistry and stable isotopes to rainfall in the QJY

Hydrochemistry and stable isotopes monitoring began at 09:30 on July 10, 2021, and ended at 07:30 on July 15, 2021, during which two rainfall events occurred. There was no rainfall for over a week before the monitoring, so the variations in the QJY were only influenced by these two rainfall events. Figure 3 shows the spring discharge, hydrochemistry and stable isotope variations in the QJY under the influence of rainfall. The first rainfall lasted from 16:30 on July 11 to 20:30 on July 11, with a cumulative rainfall of 28.8 mm and the maximum rainfall intensity was 18.2 mm/hr. After the rainfall stopped, the spring discharge began to increase and reached its peak (1763 L/s) three hours later. The second rainfall occurred from 06:30 on July 12 to 11:30 on July 12, with a cumulative rainfall of 30.2 mm. Compared with the first rainfall, the intensity of the second rainfall was more even, with the maximum intensity only 7.6 mm/hr. Four hours after the second rainfall started, the spring discharge increased again and reached the second peak (2320 l/s) 9 hours later. The spring discharge attenuation process lasted longer, and took 55 hours to return to the pre-rainfall level.

As shown in Fig. 3, the EC responded earlier than the discharge, with a rapid decline from 248 μs/cm to 217 μs/cm at the end of the first rainfall. At first, the variations of EC were exactly opposite to the discharge. With the arrival of the second rainfall, EC experienced two declines. After the EC reached its minimum, it recovered to the pre-rainfall level within 38 hours. Although the temperature of the QJY increased after the rainfall, it was not significant. The ion concentrations of Ca^{2+}, SO_4^{2-} and Sr^{2+} responded similarly to the rainfall, and they showed a peak after the rainfall started. After the first rainfall stopped for 3 hours, these ion concentrations decreased, with the Ca^{2+} concentration decreased from 45.2 mg/L to 40.9 mg/L, SO_4^{2-} decreased from 16.57 mg/L to 11.59 mg/L, and Sr^{2+} decreased from 0.312 mg/L to 0.245 mg/L. After the second rainfall occurred, they reached their minimum within 24 hours and then slowly recovered to the background values. During the whole monitoring, the concentrations of Mg^{2+}, Na^+, K^+, Cl^- and NO_3^- remained relatively stable. And it is notable that the fluctuations of K^+ and Cl^- seem to be correlated.

The temporal evolution in δD and $\delta^{18}O$ at the QJY during rainfall is shown in Fig. 3, with δD ranged from − 53.92‰ to -50.84‰ (mean value − 52.23‰) and $\delta^{18}O$ ranging from − 9.38‰ to -7.87‰ (mean value − 8.69‰). Similarly, δD decreased twice under the influence of rainfall. The first decline occurred between

the two rainfall events, from − 50.87‰ to -51.67‰. The second occurred after the second rainfall stopped for some time, after which δD remained stable. Additionally, $\delta^{18}O$ and δD decreased from − 8.03‰ to -9.38‰ after the first rainfall event, but the second decrease did not occur. Figure 4 shows the temporal variations of hydrogen and oxygen isotopes during monitoring. As time passes, the distribution of points in the vertical direction gradually moves downward, indicating that δD depleted significantly; the points are closer to each other in the horizontal direction and $\delta^{18}O$ become more concentrated. There are similar isotopic characteristics between groundwater and rainwater (δD=-63.47‰, $\delta^{18}O$=-8.65‰), suggesting that rainwater is the main source of groundwater.

5. Discussion

5.1 Identifying the structure of the QJY karst groundwater system

High-resolution monitoring can objectively reflect the response of karst groundwater systems to rainfall events and help to determine the structure of karst water system (Mohammadi et al, 2014; Chang et al, 2021). Meanwhile, continuous runoff and hydrochemistry monitoring can help us understand the relationship between hydrodynamics and hydrochemistry (Fiorillo et al, 2012; Frank et al, 2019). Especially the spring discharge, its attenuation time and characteristics are controlled by the karst development and rainfall (Bakalowicz 2005; Amiel et al, 2010). Generally, spring discharge attenuation curves can identify different medium and their proportions in karst aquifers (Jukić et al, 2015). The studies of McDonell (2003) and Peng (2012) showed that rainwater not only infiltrates through the surface but also directly enters into the ground through ponors and sinkholes and recharges groundwater. The soil thickness is relatively thin in the karst mountainous areas in Southwest China, and excessive rainwater caused by rainstorms cannot fully infiltrate into the subsurface, resulting in large amounts of surface water. This surface water is collected along the topography and gather underground through sinkholes, which provides rapid recharge (Jiang et al, 2018). In the absence of rain, spring water mainly consists of matrix flow, which is derived from the groundwater stored in the soil or fissures (Sasowsky et al, 2000; Frank et al, 2019).

The spring discharge in the QJY increases rapidly (usually within 3–7 hours) after the rainfall stops, which indicates a good connectivity from recharge area to discharge area and karst is well developed in the groundwater system. Meanwhile, the flood collected in the recharge area decreases sharply, and the spring discharge also decreases rapidly within 24 hours. There were two spring discharge attenuations at the QJY during the monitoring, and they occurred after the two rainfall events stopped. The first attenuation occurred from 22:30 on July 11 to 10:30 on July 12, and the second occurred from 15:30 on July 12 to 1:30 on July 15. Here, we focus on the more complete second attenuation, which can be obviously seen in three phases (Fig. 5).

The first phase lasted from 15:30 on July 12 to 2:30 on July 13, and the duration of this phase was very short. The spring discharge varied drastically, decreased rapidly from 2320 L/s to 1568 L/s. While Ca^{2+}, SO_4^{2-} and Sr^{2+} concentrations decreased slowly, and reached their minimum value at the end of this phase. This phase reflects the rapid transport of groundwater through well-connected pipelines, and fresh groundwater discharge before sufficient reaction of water-rock interactions. The second phase lasted from July 13, 2:30 to July 13, 18:30, with the spring discharge slowly decreased to 1026 L/s. At this time, the spring discharge was still higher than that before the rain, and the ion concentrations remained low. This phase reflects the discharge of groundwater from the wide fissures, and the water-rock interactions enter a brief state of relative equilibrium. The third phase lasted the longest, from 18:30 on July 13 to 1:30 on July 15. During this phase, spring discharge attenuated at the slowest speed and ion concentrations recovered slowly. Fissures provide better storage of groundwater, so the trailing of discharge attenuation is related to the development of fissures in the aquifers (Luo et al, 2016). In summary, the QJY karst groundwater system shows multiple medium. In addition to pipelines and wide fractures, there also exist fissures with relatively poor connectivity. Water-rock interactions are more adequate in these fissures, resulting in increases in Ca^{2+}, SO_4^{2-} and Sr^{2+} concentrations.

According to the spring discharge attenuation curve integral calculation, the accumulative discharges of the three stages were 52866m^3, 39629m^3 and 23269m^3. The results showed that groundwater from karst pipelines accounted for 45.7% of the total, while wide fissures occupied 34.2% and poorly connected fissures accounted for 20.1%.

5.2 Source of solute in groundwater

The major sources of solutes in water include rock weathering, soil leaching, atmospheric inputs and anthropogenic activities (Soulsby et al, 2007). Although the response of spring discharge indicates that groundwater primarily comes from atmospheric inputs, the influence of rock weathering on hydrochemistry is much more significant. According to the Pearson correlation analysis of hydrochemistry (Fig. 6), the following conclusions were obtained: 1, Runoff is negatively correlated with most of the indicators, indicating that the dilution effect is significant to the hydrochemistry in the QJY. 2, Ca^{2+} has a positive correlation with Mg^{2+}, HCO_3^- and Sr^{2+}, indicating that carbonate weathering dominates the hydrochemistry. 3, Sr^{2+} has a strong positive correlation with Ca^{2+}, HCO_3^- and SO_4^{2-}, suggesting that Sr^{2+} in groundwater originates from celestite and strontianite. 4, SO_4^{2-} has a positive correlation with Ca^{2+}, Sr^{2+}, HCO_3^- and Cl^-, indicating that SO_4^{2-} is probably derived from rock weathering, but cannot exclude the effects of anthropogenic pollution.

As an important alkaline soil element, Sr is sensitive to hydrological dynamics. Mineral dissolution provides Sr^{2+} to groundwater, and its concentration is determined by the groundwater residence time, so Sr can better reveal water-rock interactions (Bouchaou et al, 2008). The Sr^{2+} concentration in the QJY peaked before the first rainfall event stopped, which was faster than the response of spring discharge. Groundwater with longer residence time and more sufficient water-rock interactions had higher Sr^{2+}

concentrate. Before the first rainfall event ended, the rainwater infiltrated and pushed the groundwater stored in the surface karst zone and near-surface fissures into the pipelines. The "old groundwater" was discharged first, after which the spring discharge increased rapidly. When the spring discharge reached its maximum, the ion concentrations also reached their minimum, which was attributed to the dilution of groundwater by fresh rainwater. Continuous rainfall makes groundwater velocity faster, resulting in shorter groundwater residence time in the aquifers. Water-rock interactions were not sufficient and Sr^{2+} concentrations in the QJY decreased. It is notable that "old groundwater" was not observed during the second rainfall, and the ion concentrations continued to decline. After the rainfall stopped, the ion concentrations slowly recovered to the background values within 72 hours. During the recovery process, the variations of Sr^{2+} concentrate showed opposite characteristics to the spring discharge. Obviously, the recovery time of Sr^{2+} concentration from the minimum to the background value almost coincided with the third phase of the spring discharge attenuation.

The studies of (Agrawal et al, 1999; Jeong 2001) showed that Cl^- and NO_3^- originated from agricultural activities remained in the soil and rainwater leached and recharged to groundwater. There was no significant correlation between Cl^- and NO_3^- in the QJY, while Cl^- and K^+ showed a stronger correlation. Previous studies have reported the presence of sylvite in the evaporite strata of the study area, and it is inferred that sylvite provides Cl^- to the groundwater (Li 1988). However, Cl^- and K^+ only fluctuated during rainfall, indicated that the dissolution velocity of sylvite did not vary with hydrodynamics.

The δD in groundwater showed a decreasing trend and converged to rainfall (δD = -63.47‰), which indicated that rainfall has a great influence on groundwater. Carbonate rocks are oxygen-rich rocks, and groundwater is enriched in $\delta^{18}O$ after flowing through carbonate rocks, but δD does not vary appreciably (Luo et al, 2016). When rainwater infiltrates underground, fresh groundwater dissolves the minerals in the aquifers. Simultaneously, isotopic fractionation occurs between groundwater and karst aquifers. Therefore, the $\delta^{18}O$ in groundwater of the QJY increased after both rainfall events.

5.3 Evolution of water-rock interactions during rainfall

The previous analysis showed that the QJY karst water system has multiple mediums, which correspond to different groundwater residence times. Climate altered groundwater flow paths, so spring discharge and hydrochemistry reflected groundwater from different mediums with time (Lee et al, 2001). Besides, precipitation and recharge also affect the hydrogeochemical processes that occurred in the aquifers (Musgrove et al, 2010).

The saturation indexes of calcite, dolomite, gypsum, celestite and strontianite were calculated to illustrate the hydrogeochemical processes and water-rock interactions occurred in the groundwater, and the results are shown in Fig. 7. In general, calcite dissolved "supersaturated"; dolomite dissolved "supersaturated" or in equilibrium; gypsum, celestite and strontianite dissolved "unsaturated". According to the variations of the saturation index, the hydrogeochemical processes exhibited three stages. The first stage occurred before the rainfall, calcite and dolomite were in the dissolved "supersaturation" state, and the saturation

indexes were relatively stable. The second stage is between the two peaks of the spring discharge in the QJY. Calcite dissolved "supersaturated", and the saturation indexes decreased; dolomite dissolved in equilibrium; gypsum and celestite dissolved "unsaturated", with the saturation index increased. The groundwater gradually recovered in the third stage, with the saturation indexes of calcite and dolomite increased, gypsum and celestite decreased. Calcite, dolomite and gypsum dissolved faster in the second stage, while it slowed down in the third stage.

The spring is in low-flow conditions before the rainfall began, and most of the groundwater stored in the fissures is discharged through the pipelines. The piston effect occurs first at the beginning of the rainfall. When the rainwater infiltrates, groundwater in the fissures of the surface karst zone is pushed into the pipelines. In addition, rainwater dissolves carbon dioxide in the soil, which leads to a decrease in pH as well as an increase in mineral solubility (Liu et al, 2004). It was observed that the pH decreased from 8.13 to 8.07 after the rainfall began, which supported the contribution of soil CO_2. Therefore, both "old groundwater" and soil CO_2 may lead to the peak in ion concentrations. Furthermore, the water-rock interactions experienced unexpected alterations under the influence of the rainfall. Although solutes in groundwater were controlled by the dissolution of carbonate minerals, the variations in hydrochemistry caused by rainfall were mainly derived from gypsum (one of the evaporite minerals). The spring discharge increased tens of time, while the ion concentrations decreased by only one-tenth, which indicated that the minerals continued to dissolve and became faster as the spring discharge increased. Runoff is one of the most important factors affecting mineral dissolution, but the speed of mineral dissolution does not increase indefinitely. When the runoff exceeds a threshold value, the dilution effect begins to be significant.

5.4 Mixing calculations for different sources

The ion concentrations vary continuously with time under the influence of rainfall, which implies that groundwater from different sources also changes (Liu et al, 2004). The sources of solutes in the QJY include rains, carbonate rock and evaporites (gypsum and sylvite), and their contributions to the dissolved loads are calculated by the mass conservation equations. In contrast to the research of (Moon et al, 2007), silicate rocks have less influence on solute and therefore were not considered. Because Na is not susceptible to nutrient cycling in ecosystems, the selected ions were Na-normalized to eliminate the effects of runoff and evaporation (Millot et al, 2003). However, K^+ and SO_4^{2-} in the QJY mainly originate from evaporites and are affected less by biological activity, so the mass conservation equations include K^+ and SO_4^{2-}. We simplified these equations (Eq. (2)-Eq. (8)) to reduce the errors in the calculation results caused by ions at lower concentrations. Where x_i denotes the mixing proportion of Na from different sources (rain, carbonate and evaporite).

$$\left(\frac{Ca}{Na}\right)_{groundwater}=\left(\frac{Ca}{Na}\right)_{rain}x_{rain}+\left(\frac{Ca}{Na}\right)_{carbonate}x_{carbonate}+\left(\frac{Ca}{Na}\right)_{evaporite}x_{evaporite}\text{Eq.(2)}$$

$$\left(\frac{Mg}{Na}\right)_{groundwater}=\left(\frac{Mg}{Na}\right)_{rain}x_{rain}+\left(\frac{Mg}{Na}\right)_{carbonate}x_{carbonate}\ \text{Eq.(3)}$$

$$\left(\frac{K}{Na}\right)_{groundwater}=\left(\frac{K}{Na}\right)_{rain}x_{rain}+\left(\frac{K}{Na}\right)_{evaporite}x_{evaporite}\text{Eq.(4)}$$

$$\left(\frac{HCO_3}{Na}\right)_{groundwater}=\left(\frac{HCO_3}{Na}\right)_{rain}x_{rain}+\left(\frac{HCO_3}{Na}\right)_{carbonate}x_{carbonate}\text{Eq.(5)}$$

$$\left(\frac{SO_4}{Na}\right)_{groundwater}=\left(\frac{SO_4}{Na}\right)_{rain}x_{rain}+\left(\frac{SO_4}{Na}\right)_{evaporite}x_{evaporite}\text{Eq.(6)}$$

$$\left(\frac{Cl}{Na}\right)_{groundwater}=\left(\frac{Cl}{Na}\right)_{rain}x_{rain}+\left(\frac{Cl}{Na}\right)_{evaporite}x_{evaporite}\text{Eq.(7)}$$

$$\sum(x)_i=1\text{Eq.(8)}$$

In this approach, all parameters are considered to be unknown. A set of a priori parameters values was chosen to constrain different sources. Some of these parameters for the carbonate and evaporite were obtained from (Millot et al, 2003; Chetelat et al, 2008; Zhang et al, 2021). The rainwater collected in this monitoring was used as the parameters for rain. The parameters $(Z/Na)_i$ (Z = Ca, Mg, K, HCO_3, SO_4, Cl) and x_i from different sources were solved by the commercial version of 1stopt 9.0 software. The inversion of the parameters was based on 511 equations, which contained 6*73 mass balance equations of constant elements and 73 isotope constraint equations. After a series of successive iterations, 219 x_i and 13 $(Z/Na)_i$ were obtained as the optimal solutions (Table 1).

To test the sensitivity of the inverse calculation, we changed the prior range. Two scenarios were set up in the sensitivity test of the rain parameters: (1) rainwater collected in the city near the QJY on August 9, 2020; (2) rainwater collected in this monitoring. The contributions of rain (x_{rain}) to the dissolved cations were 7.3% (1.9%-15%) and 5.0% (0.1%-10.4%) in these two scenarios. Scenario 2 was chosen for the final run after optimization. Another sensitivity test for carbonate was set up with two scenarios: (3) with Mg/Na ranging from 12 to 28, which was referenced from numerous studies (Millot et al, 2003; Moon et al, 2007); (4) another scenario was chosen for a wider range of Mg/Na, from 7 to 28. These two scenarios exhibited similar calculations, with the contribution of carbonate weathering ($x_{carbonate}$) were 83.4% (85.2%-80.3%) and 81.5% (86.0-%79.0%). Considering the hydrogeochemical characteristics of the QJY, we believe that Scenario 3 is more suitable for this study. Blind use of the inversion calculations may

produce erroneous results. However, the sensitivity test helps us to obtain accurate results by reducing the uncertainty of background information.

Table 1
The priori ranges and the optimal posterior values for each parameter in the inverse calculation

the priori ranges	Ca/Na	Mg/Na	K/Na	HCO_3/Na	SO_4/Na	Cl/Na
Rain	3.173	0.087	1.616	6.573	2.066	1.544
Carbonate	40–50	7–28	-	40–120	-	-
Evaporite	5–10	-	0.5-9	-	5–10	0.5-9
the posteriori values						
Rain	3.173	0.087	1.616	6.573	2.066	1.544
Carbonate	43.735	6.815	-	104.470	-	-
Evaporite	8.852	-	2.518	-	7.987	1.956

The contributions of rain, carbonate and evaporite to dissolved cations are shown in Fig. 8. Moreover, carbonate weathering is the dominant source, accounting for 83.4% (85.2%-80.3%). With respect to the other two sources, the contribution of rain is 5.0% (0.1%-10.4%) and evaporite weathering is 11.6% (6.9%-18.0%). Although rainwater provides large amounts of groundwater to the QJY karst water system, it contributes little to the solutes. This is attributed to the lower ion concentration in the rainwater. The results show that rain contributes only 2.6 – 0.2% to the dissolved cations in the early stages of the rainfall. As the dilution effect becomes significant, the contribution of rain increases to 7.2%.

During the evolution of hydrochemistry and spring discharge, the contribution of evaporites to dissolved cations varied, while carbonates did not vary markedly. Coincidentally, the contribution of evaporite to dissolved cations varied with the process of different phases. The proportion of evaporite stabilized at 14.5% (12.3% ~ 16.6%) before rainfall and increased to 17.0% (14.3% ~ 18.0%) thereafter. It seemed that the percentage of evaporites decreased as the spring discharge increased. When the spring discharge attenuated to the pre-rainfall level, the contribution of evaporite also recovered. This implies that evaporite weathering may be controlled by the medium. Groundwater flows more fluently in the pipelines and wide fissures, which allows adequate dissolution of soluble evaporite minerals on the rock surface. Therefore, evaporite is relatively absent in these mediums. Whereas, the proportion of the matrix flow in the QJY is higher in the low-flow conditions, and evaporite contributes more to dissolved cations.

5.5 Hydrogeochemical conceptual model

The results of the study present a conceptual model of hydrogeochemistry. It summarizes the hydrogeochemical processes and different solute sources in a typical karst groundwater system

evaporite minerals after being recharged by pulsed rainfall. Different mediums and groundwater flow characteristics in them are important factors in the hydrogeochemical evolution. The conceptual model is divided into three phases.

In the absence of rain, the spring is in low-flow conditions (Fig. 9a). In such conditions, the hydraulic head of the pipeline is lower than the surrounding matrix. Therefore, the spring discharge is mainly composed of matrix flow at this time, i. e., groundwater in the fissures. Water-rock interactions are more adequate in the fractures, and also provide abundant dissolved ions for groundwater. The concentrations of Ca^{2+}, HCO_3^- and SO_4^{2-} in the spring remained high, which indicated that calcite and gypsum were the main sources of solutes in the groundwater. Furthermore, carbonate minerals dissolved "supersaturated", gypsum dissolved, and the contribution of rock weathering to dissolved cations remained stable.

The fast response of the spring after pulsed rainfall indicates that groundwater flows unimpeded in the karst water system. The spring is a mixture of three water types: groundwater originally stored in the fissures, rainwater directly injected into the ground through the ponor, and "new groundwater" recharged to the fissures by rainwater. The proportion of different water types varies accordingly, which is the fundamental cause of the variation in hydrochemistry. Before the spring reaches high-flow conditions, it first experiences the " old groundwater" discharge phase (Fig. 9b). Fresh rainwater infiltrates underground and pushes groundwater previously stored in fissures into the pipelines, also known as the piston effect. This results in a sudden increase in Ca^{2+}, SO_4^{2-} and Sr^{2+} concentrations during the early rainfall events. Apparently, the variations in hydrochemistry in these circumstances are mainly caused by gypsum and celestite. The contribution of evaporite weathering to dissolved cations also increases. While the carbonate minerals are still dissolved "supersaturated". This means that in such karst aquifers with evaporite minerals, the amount of gypsum dissolved in groundwater is the main difference between "old groundwater" and "new groundwater".

In high-flow conditions (Fig. 9c), the hydraulic head in the pipeline is higher than the surrounding matrix as fresh groundwater continues to sink into the pipeline. Groundwater transports along the direction of the pipeline development and spring discharge increases rapidly. Water-rock interactions are more intense than other times. The dissolution of carbonate minerals is the dominant hydrogeochemical process, which may be responsible for maintaining carbonate weathering to remain stable. However, the maximum intensity restricts the ion concentration, which results in lower ion concentrations in groundwater under the diluting effect of "fresh water". Meanwhile, the contribution of rain to dissolved cations increases slightly. It is possible that strong runoff can dissolve soluble minerals around the pipelines in high-flow conditions. Therefore, gypsum and other soluble minerals are relatively absent in the pipelines, which is one of the reasons for the reduction in the proportion of evaporite weathering.

Conclusion

High-resolution monitoring was conducted in the QJY, a karst groundwater source in Hubei, China. A combination of runoff, hydrochemistry, and stable isotopes was used in this study to explore the

response of the karst water system to rainfall. The advances in the study support a hydrogeological conceptual model that explains the observed hydrogeochemical behavior.

The results show that (1) the spring discharge attenuation curve can be divided into three phases, which indicates the development of multiple mediums in the aquifer. (2) As the spring discharge increased, the intensity of water-rock interactions also enhanced, but not indefinitely. (3) A more important finding is that carbonate minerals provide large amounts of solutes to groundwater, but the variations in hydrochemistry caused by rainfall are associated with gypsum and celestite dissolution. (4) The dissolution of gypsum may be related to the residence time of groundwater, and in the karst aquifers with evaporite minerals, the amount of gypsum dissolved in the groundwater is the main difference between "old groundwater" and "new groundwater". The source of SO_4^{2-} was distinguished during the study and is mainly controlled by dissolution of sulfur-containing minerals rather than anthropogenic activities. Although carbonate minerals provide large amounts of solutes to groundwater. Gypsum, as a less abundant mineral, needs to be further investigated for its importance in the karst aquifers.

Declarations

Authors' contributions

Xinhui He: Conceptualization, Methodology, Data collation, Visualization, Writing-original draft. **Zhou Hong**: Project administration, Supervision, Methodology. **Junwei Wan**: Conceptualization, Supervision, Writing-review and editing. **Yuan Guo**: Investigation, Resources, Data curation. **Heng Zhao**: Investigation, Resources, Data curation.

Acknowledgments This study was supported by a project of the China Geological Survey (DD20190824) and the National Key Research and Developmental Program of China (2016YFC0502302). Our special thanks are given to Li Wan, Zhenyu Ni, Yulin Deng and Xiangyong Chen for their help with field and laboratory work.

Availability of data and materials Data available on request due to restrictions e.g., privacy or ethical.

Ethics approval Not applicable.

Consent to participate Not applicable.

Consent for publication Not applicable.

Competing interests The authors declare no competing interests.

References

1. Agrawal GD, Lunkad SK, Malkhed T (1999) Diffuse agricultural nitrate pollution of groundwaters in India. Water Sci Technol 39:67–75. https://doi.org/10.1016/S0273-1223(99)00033-5

2. Amiel RB, Grodek T, Frumkin A (2010) Characterization of the hydrogeology of the sacred Gihon Spring, Jerusalem: a deteriorating urban karst spring. Hydrogeol J 18:1465–1479. https://doi.org/10.1007/s10040-010-0600-6
3. Bakalowicz M (2005) Karst groundwater: a challenge for new resources. Hydrogeol J 13:148–160. https://doi.org/10.1007/s10040-004-0402-9
4. Bouchaou L, Michelot J, Vengosh A, Hsissou Y, Mohamed Q, Gaye C, Bullen T, Zuppi G (2008) Application of multiple isotopic and geochemical tracers for investigation of recharge, salinization, and residence time of water in the Souss–Massa aquifer, southwest of Morocco. J Hydrology 352:267–287. https://doi.org/10.1016/j.jhydrol.2008.01.022
5. Chang W, Wan JW, Tan JH, Wang ZX, Jiang C, Huang K (2021) Response of spring discharge to different rainfall events for single-conduit karst aquifers in western Hunan Province, China. Int J Environ Res Public Health 18. https://doi.org/10.3390/ijerph18115775
6. Chen H, Xiang TT, Zhou X, Xu CY (2012) Impacts of climate change on the Qingjiang Watershed's runoff change trend in China. Stoch Environ Res Risk Assess 26:847–858. https://doi.org/10.1007/s00477-011-0524-2
7. Chetelat B, Liu CQ, Zhao ZQ, Wang QL, Li SL, Li J, Wang BL (2008) Geochemistry of the dissolved load of the Changjiang Basin rivers: Anthropogenic impacts and chemical weathering. Geochim Cosmochim Acta 72:4254–4277. https://doi.org/10.1016/j.gca.2008.06.013
8. Darling WG, Bowes MJ (2016) A long-term study of stable isotopes as tracers of processes governing water flow and quality in a lowland river basin: the upper Thames, UK. Hydrol Process 30:2178–2195. https://doi.org/10.1002/hyp.10779
9. Doctor DH Jr, Petrič ECA, Kogovšek M, Urbanc J, Lojen J, Stichler S W (2006) Quantification of karst aquifer discharge components during storm events through end-member mixing analysis using natural chemistry and stable isotopes as tracers. Hydrogeol J 14:1171–1191. https://doi.org/10.1007/s10040-006-0031-6
10. Fiorillo F, Guadagno FM (2012) Long karst spring discharge time series and droughts occurrence in Southern Italy. Environ Earth Sci 65:2273–2283. https://doi.org/10.1007/s12665-011-1495-9
11. Frank S, Goeppert N, Ohmer M, Goldscheider N (2019) Sulfate variations as a natural tracer for conduit-matrix interaction in a complex karst aquifer. Hydrol Process 33:1292–1303. https://doi.org/10.1002/hyp.13400
12. Gassen N, Griebler C, Werban U, Trauth N, Stumpp C (2017) High resolution monitoring above and below the groundwater table uncovers small-scale hydrochemical gradients. Environ Sci Technol 51:13806–13815. https://doi.org/10.1021/acs.est.7b03087
13. Herman EK, Toran L, White WB (2009) Quantifying the place of karst aquifers in the groundwater to surface water continuum: A time series analysis study of storm behavior in Pennsylvania water resources. J Hydrology 376:307–317. https://doi.org/10.1016/j.jhydrol.2009.07.043
14. Hu CH, Hao YH, Yeh TJ, Pang B, Wu ZN (2008) Simulation of spring flows from a karst aquifer with an artificial neural network. Hydrol Processes 22:596–604. https://doi.org/10.1002/hyp.6625

15. Jeong CH (2001) Effect of land use and urbanization on hydrochemistry and contamination of groundwater from Taejon area, Korea. J Hydrology 253:194–210. https://doi.org/10.1016/S0022-1694(01)00481-4
16. Jiang YJ, Cao M, Yuan DX, Zhang YZ, He QF (2018) Hydrogeological characterization and environmental effects of the deteriorating urban karst groundwater in a karst trough valley: Nanshan, SW China. Hydrogeol J 26:1487–1497. https://doi.org/10.1007/s10040-018-1729-y
17. Jukić D, Denić-jukić V (2015) Investigating relationships between rainfall and karst-spring discharge by higher-order partial correlation functions. J Hydrology 530:24–36. https://doi.org/10.1016/j.jhydrol.2015.09.045
18. Kurtulus B, Razack M (2010) Modeling daily discharge responses of a large karstic aquifer using soft computing methods: Artificial neural network and neuro-fuzzy. J Hydrology 381:101–111. https://doi.org/10.1016/j.jhydrol.2009.11.029
19. Lee ES, Krothe NC (2001) A four-component mixing model for water in a karst terrain in south-central Indiana, USA. Using solute concentration and stable isotopes as tracers. Chem Geol 179:129–143. https://doi.org/10.1016/S0009-2541(01)00319-9
20. Li JH, Qi YQ, Zhong Y, Yang LH, Xu YQ, Lin P, Wang SF, He J (2016) Karst aquifer characterization using storm event analysis for Black Dragon springshed, Beijing, China. CATENA 145:30–38. https://doi.org/10.1016/j.catena.2016.05.019
21. Li SR (1988) The tectonic factors conducive to the formations of evaporites during the Indosinian in Hubei province and its adjacent areas are discussed.Acta Geologica Sinica:123–130. https://kns.cnki.net/kcms/detail/detail.aspx?FileName=DZXE198802002&DbName=CJFQ1988 (in Chinese)
22. Li YQ, Li SJ, He DF, Gao J, Wang YC, Huang HY, Zhang JT, Zhang Y (2020) Middle Triassic tectono-sedimentary development of Sichuan Basin: Insights into the cratonic differentiation. Geol J 56:1858–1878. https://doi.org/10.1002/gj.4033
23. Liu ZH, Groves C, Yuan DX, Meiman J, Jiang GH, He SY, Li Q (2004) Hydrochemical variations during flood pulses in the south-west China peak cluster karst: impacts of $CaCO_3$-H_2O-CO_2 interactions. Hydrol Process 18:2423–2437. https://doi.org/10.1002/hyp.1472
24. Luo MM, Chen ZH, Criss RE, Zhou H, Huang H, Han ZF, Shi TT (2016) Dynamics and anthropogenic impacts of multiple karst flow systems in a mountainous area of South China. Hydrogeol J 24:1993–2002. https://doi.org/10.1007/s10040-016-1462-3
25. Luo MM, Chen ZH, Yin DC, Jakada H, Huang H, Zhou H, Wang T (2016) Surface flood and underground flood in Xiangxi River Karst Basin: Characteristics, models, and comparisons. J Earth Sci 27:15–21. https://doi.org/10.1007/s12583-016-0624-5
26. Luo MM, Chen ZH, Zhou H, Jakada H, Zhang L, Han ZF, Shi TT (2016) Identifying structure and function of karst aquifer system using multiple field methods in karst trough valley area, South China. Environ Earth Sci 75:824. https://doi.org/10.1007/s12665-016-5630-5

27. Luo MM, Chen ZH, Zhou H, Zhang L, Han ZF (2017) Hydrological response and thermal effect of karst springs linked to aquifer geometry and recharge processes. Hydrogeol J 26:629–639. https://doi.org/10.1007/s10040-017-1664-3
28. McDonell JJ (2003) Where does water go when it rains? Moving beyond the variable source area concept of rainfall-runoff response. Hydrol Processes 17:1869–1875. https://doi.org/10.1002/hyp.5132
29. Meredith KT, Hollins S, Hughes CE, Cendón DI, Hankin S, Stone D (2009) Temporal variation in stable isotopes (^{18}O and ^{2}H) and major ion concentrations within the Darling River between Bourke and Wilcannia due to variable flows, saline groundwater influx and evaporation. J Hydrology 378:313–324. https://doi.org/10.1016/j.jhydrol.2009.09.036
30. Millot R, Gaillardet J, Dupré B, Allègre CJ (2003) Northern latitude chemical weathering rates: clues from the Mackenzie River Basin, Canada. Geochimica et Cosmochimica Acta. 67:1305–1329. https://doi.org/10.1016/S0016-7037(02)01207-3
31. Mohammadi Z, Shoja A (2014) Effect of annual rainfall amount on characteristics of karst spring hydrograph. Carbonates and Evaporites 29:279–289. https://doi.org/10.1007/s13146-013-0175-0
32. Moon S, Huh Y, Qin JH, Pho NV (2007) Chemical weathering in the Hong (Red) River basin: Rates of silicate weathering and their controlling factors. Geochim et Cosmochim Acta 71:1411–1430. https://doi.org/10.1016/j.gca.2006.12.004
33. Musgrove M, Stern L, Banner JL (2010) Springwater geochemistry at Honey Creek State Natural Area, central Texas: Implications for surface water and groundwater interaction in a karst aquifer. J Hydrology 388:144–156. https://doi.org/10.1016/j.jhydrol.2010.04.036
34. Nisi B, Buccianti A, Vaselli O, Perini G, Tassi F, Minissale A, Montegrossi G (2008) Hydrogeochemistry and strontium isotopes in the Arno River Basin (Tuscany, Italy): Constraints on natural controls by statistical modeling. J Hydrology 360:166–183. https://doi.org/10.1016/j.jhydrol.2008.07.030
35. Peng T, Wang SJ (2012) Effects of land use, land cover and rainfall regimes on the surface runoff and soil loss on karst slopes in southwest China. CATENA 90:53–62. https://doi.org/10.1016/j.catena.2011.11.001
36. Perrin J, Jeannin P, Zwahlen F (2003) Implications of the spatial variability of infiltration-water chemistry for the investigation of a karst aquifer: a field study at Milandre test site, Swiss Jura. Hydrogeol J 11:673–686. https://doi.org/10.1007/s10040-003-0281-5
37. Pu JB, Yuan DX, He QF, Wang ZJ, Hu ZY, Gou PF (2011) High-resolution monitoring of nitrate variations in a typical subterranean karst stream, Chongqing, China. Environ Earth Sci 64:1985–1993. https://doi.org/10.1007/s12665-011-1019-7
38. Sasowsky ID, Wicks CM (2000) Groundwater flow and contaminant transport in carbonate aquifers. Taylor & Francis, pp 113–128
39. Soulsby C, Tetzlaff D, Bedem NVD, Malcolm I, Bacon PJ, Youngson AF (2007) Inferring groundwater influences on surface water in montane catchments from hydrochemical surveys of springs and streamwaters. J Hydrology 333:199–213. https://doi.org/10.1016/j.jhydrol.2006.08.016

40. Sun J, Yoshio T, William HS, Toshihiro K, Wang B, Wu P, Zhu LJ, Dong ZF (2021) Identification and quantification of contributions to karst groundwater using a triple stable isotope labeling and mass balance model. Chemosphere 263:127946. https://doi.org/10.1016/j.chemosphere.2020.127946
41. Sun Y, Wan JW, Yang SY, Xue XH, Huang K (2016) Influences of water conservancy and hydropower projects on runoff in Qingjiang River Upstream Basin. J Earth Sci 27:110–116. https://doi.org/10.1007/s12583-016-0640-5
42. Wang JJ, Liang X, Ma B, Liu YF, Jin MG, Peter SKK, Liu YL (2021) Using isotopes and hydrogeochemistry to characterize groundwater flow systems within intensively pumped aquifers in an arid inland basin, Northwest China. J Hydrology 595:126048. https://doi.org/10.1016/j.jhydrol.2021.126048
43. Wang ZJ, Guo XL, Kuang Y, Chen QL, Luo MM, Zhou H (2022) Recharge sources and hydrogeochemical evolution of groundwater in a heterogeneous karst water system in Hubei Province, Central China. Appl Geochem 136:105165. https://doi.org/10.1016/j.apgeochem.2021.105165
44. Wang ZX, Wu R, Huang K, Qiu Y, Li ZX, Lv Y, Wan JW (2021) Structure identification of a karst groundwater system based on high-resolution rainfall-hydrological response characteristics. Environ Sci Pollut Res. https://doi.org/10.1007/s11356-021-17880-x
45. White WB (2002) Karst hydrology: recent developments and open questions. Eng Geol 65:85–105. https://doi.org/10.1016/S0013-7952(01)00116-8
46. Xu RC, Yan FZ (2004) Karst geology and engineering treatment in the Geheyan Project on the Qingjiang River. China Eng Geol 76:155–164. https://doi.org/10.1016/j.enggeo.2004.06.012
47. Zhang X, Xu ZF, Liu WJ, Moon S, Zhao T, Zhou XD, Zhang JY, Wu Y, Jiang H, Zhou L (2019) Hydrogeochemical and Sr isotopic characteristics of the Yalong River Basin, eastern Tibetan Plateau: implications for chemical weathering and controlling factors. Geochem Geophys Geosyst 20:1221–1239. https://doi.org/10.1029/2018GC007769
48. Zhang Y, Yu S, He SY, Sun PA, Wu F, Liu ZY, Zhu HY, Li X, Zeng P (2021) New estimate of chemical weathering rate in Xijiang River Basin based on multi-model. Sci Rep 11:5728. https://doi.org/10.1038/s41598-021-84602-1
49. Zhao M, Zeng C, Liu ZH, Wang SJ (2010) Effect of different land use/land cover on karst hydrogeochemistry: A paired catchment study of Chenqi and Dengzhanhe, Puding, Guizhou, SW China. J Hydrology 388:121–130. https://doi.org/10.1016/j.jhydrol.2010.04.034
50. Zhou Q, Chen L, Singh VP, Zhou JZ, Chen XH, Xiong LH (2019) Rainfall-runoff simulation in karst dominated areas based on a coupled conceptual hydrological model. J Hydrology 573:524–533. https://doi.org/10.1016/j.jhydrol.2019.03.099

Figures

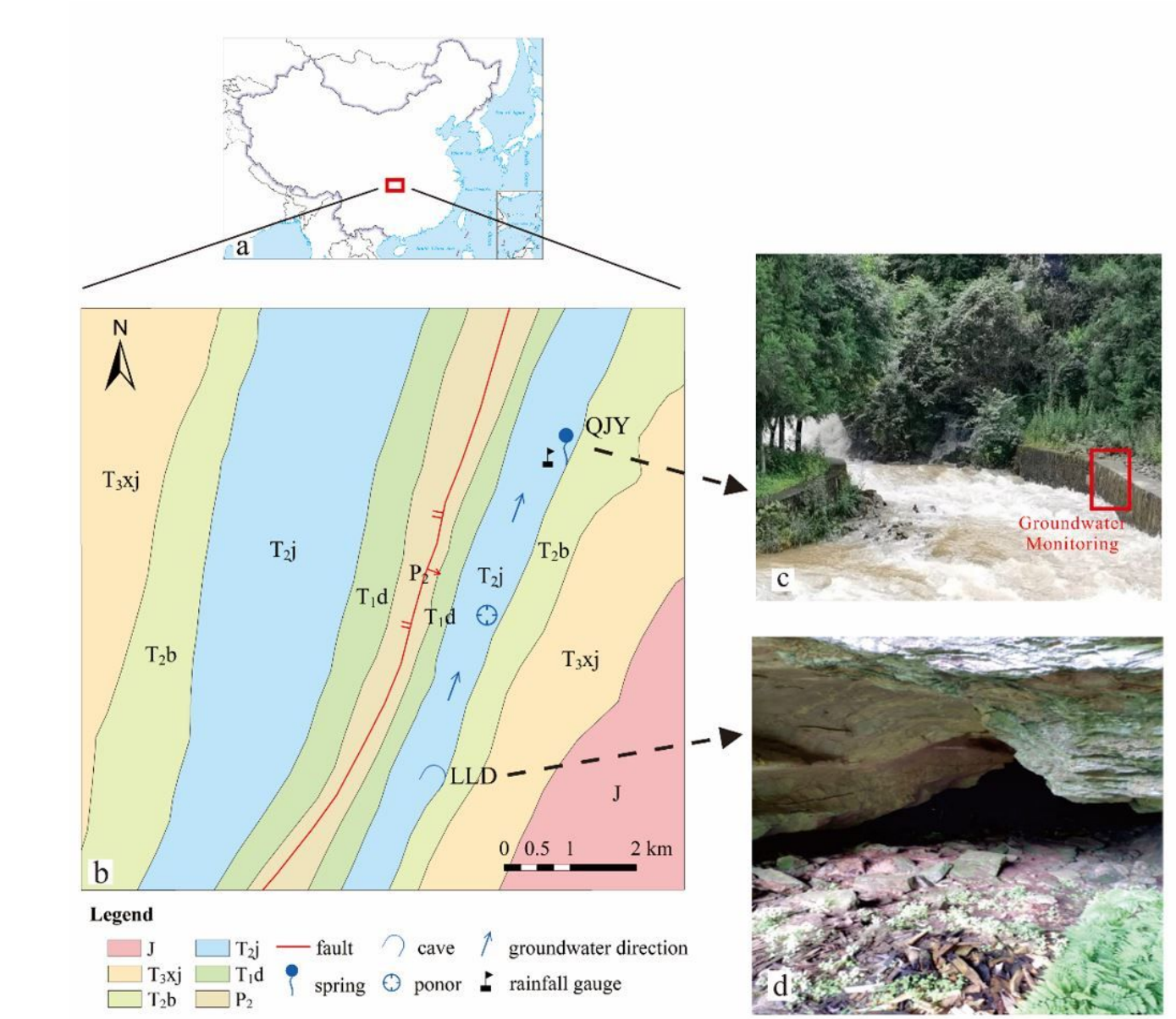

Figure 1

a Geographic location of the study area in China; **b** Hydrogeological map of the study area; **c** Spring export and groundwater monitoring in the QJY; **d** LLD, one of the entrances of the QJY

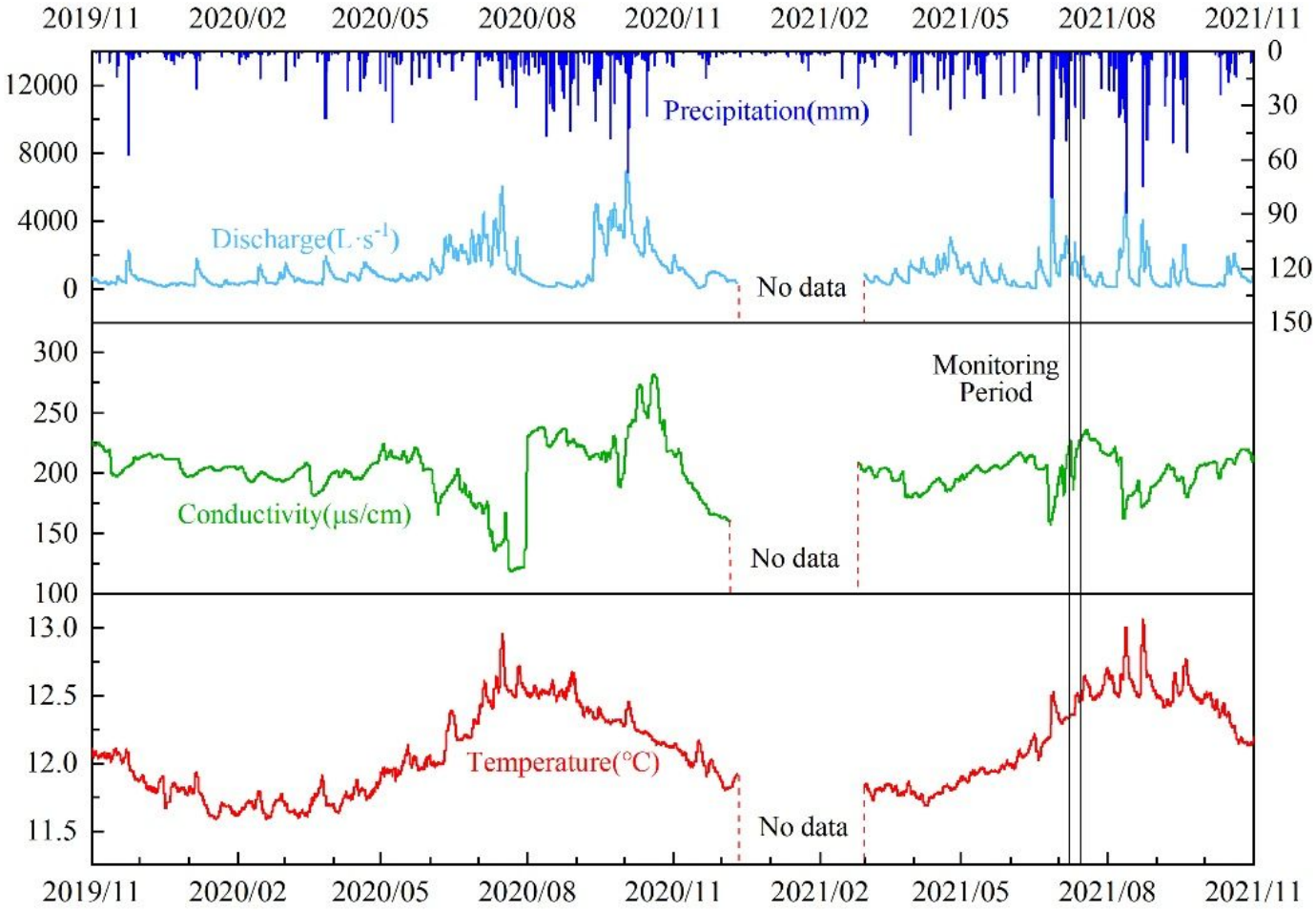

Figure 2

Spring discharge, temperature and electrical conductivity (EC) curves of the QJY

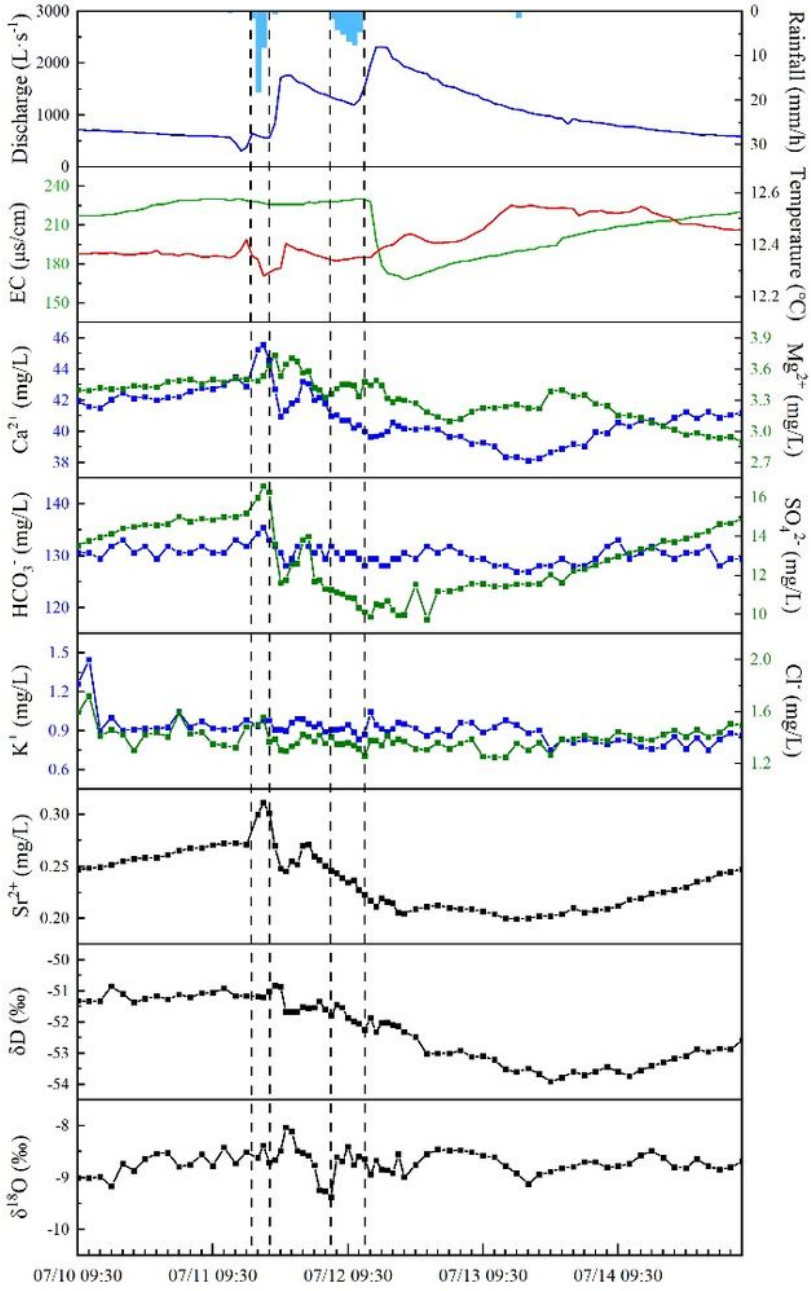

Figure 3

Rainfall, discharge, EC, temperature, ion concentrations, δD and $\delta^{18}O$ of the QJY

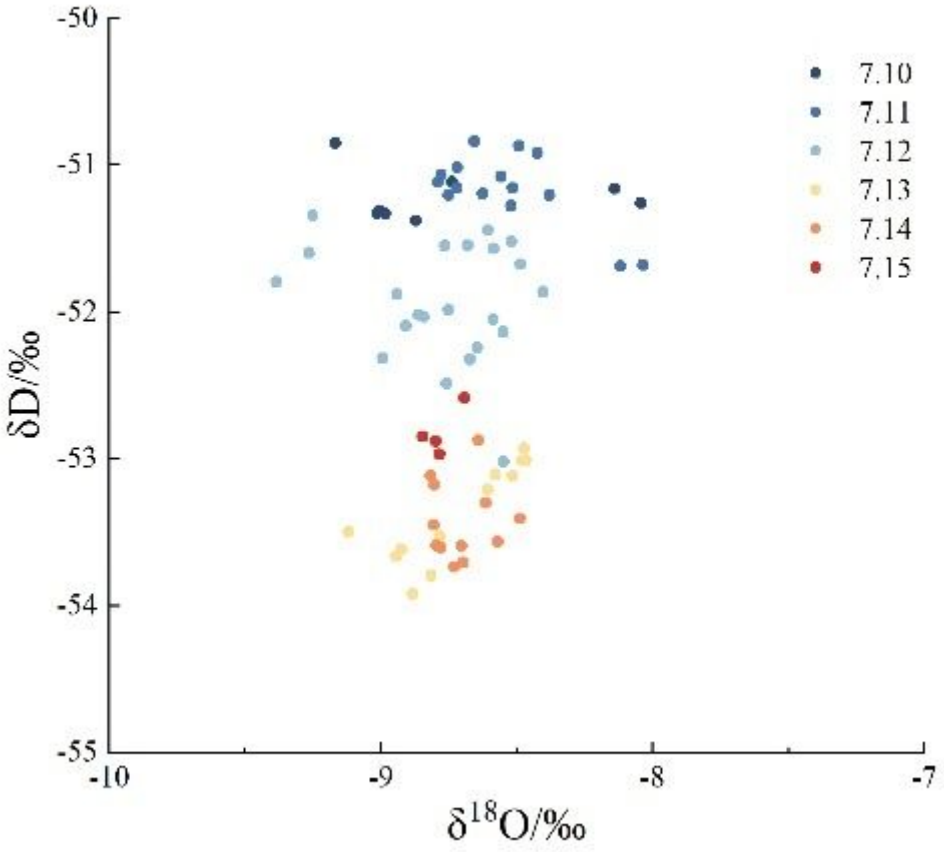

Figure 4

Plots of δD vs. $\delta^{18}O$ in the QJY, and points change from blue to red with time

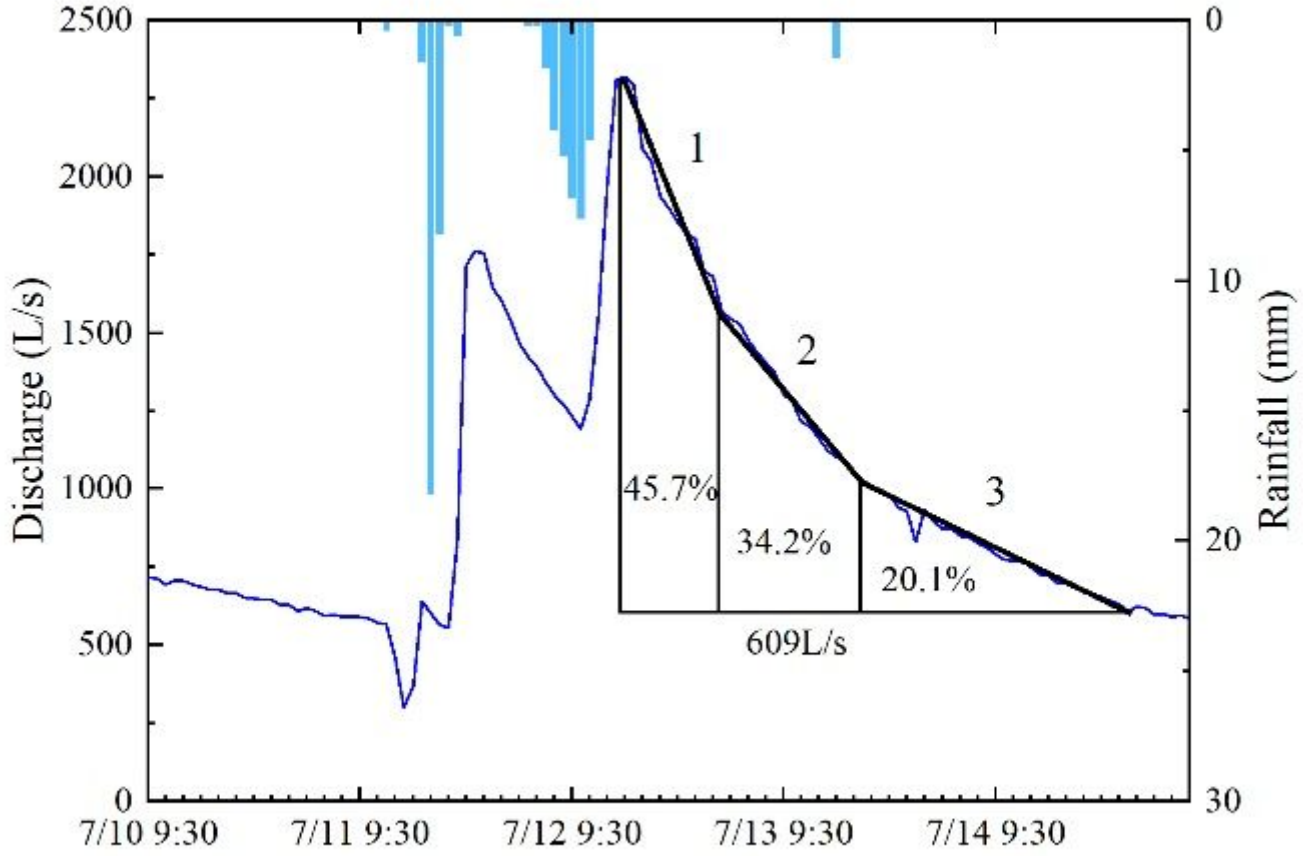

Figure 5

Spring discharge attenuation curve in the QJY (2021.7.10 9:30-2021.7.14 7:30)

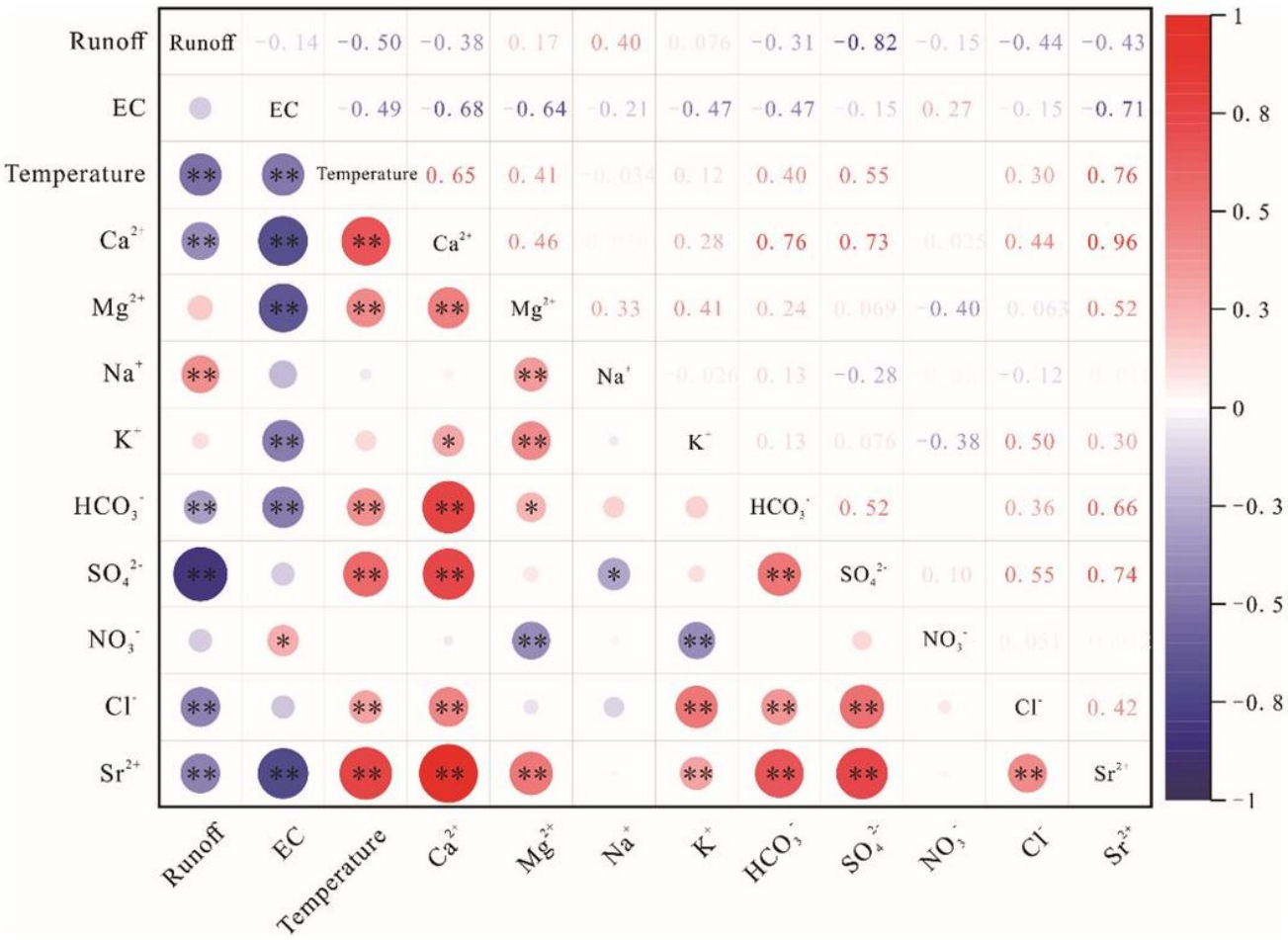

Figure 6

Heatmap of the correlation coefficient matrix (*p≤0.05 and **p≤0.01)

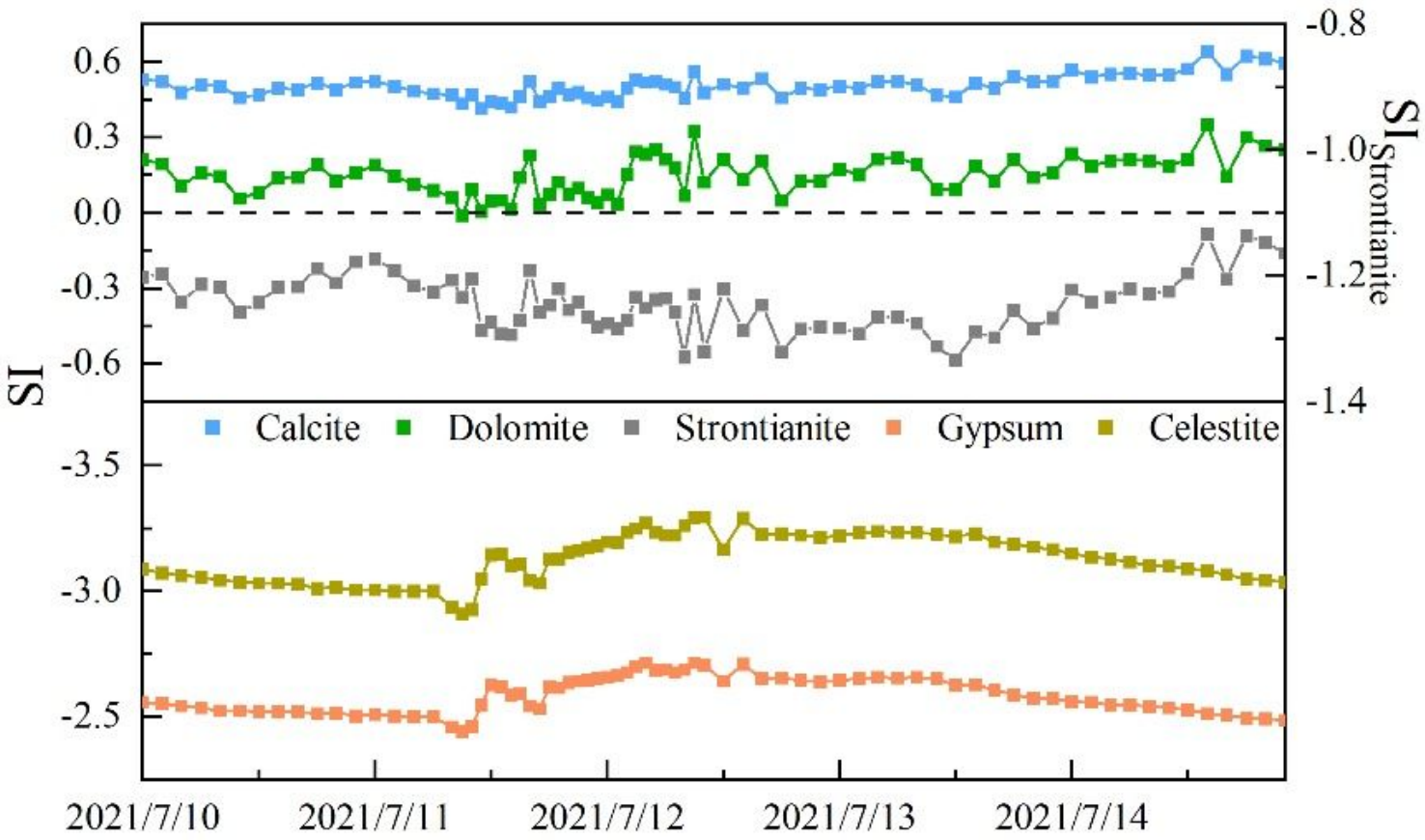

Figure 7

Saturation index of calcite, dolomite, gypsum, celestite and strontianite in the QJY

Figure 8

The contributions of different sources to the dissolved cations in the QJY

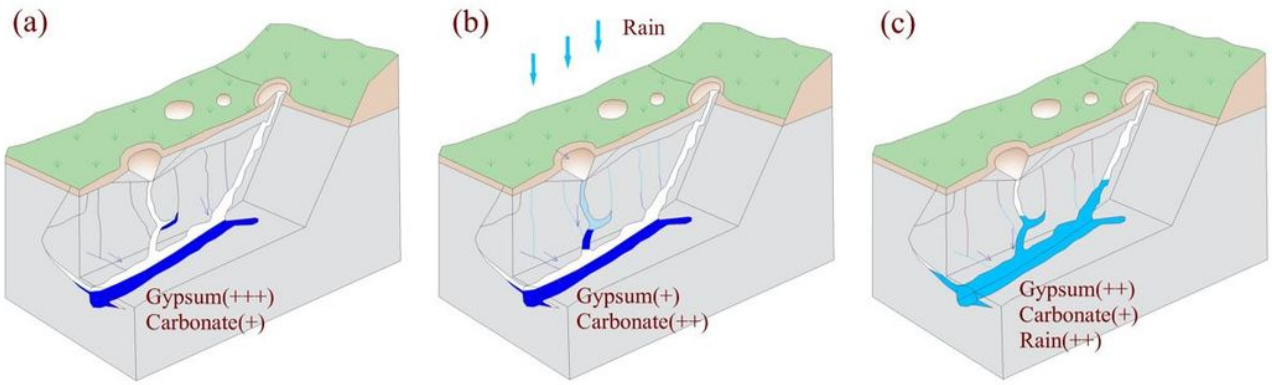

Figure 9

Hydrogeochemical conceptual model for the karst water system contained gypsum minerals at different phases